

# 1 MW J-PARC RCS BEAM OPERATION AND FURTHER BEYOND

H. Hotchi<sup>1†</sup>, H. Harada<sup>2</sup>, N. Hayashi<sup>2</sup>, M. Kinsho<sup>2</sup>, K. Okabe<sup>2</sup>, P.K. Saha<sup>2</sup>, Y. Shobuda<sup>2</sup>,  
 F. Tamura<sup>2</sup>, K. Yamamoto<sup>2</sup>, M. Yamamoto<sup>2</sup> and M. Yoshimoto<sup>2</sup>  
 Accelerator Division, J-PARC Center, <sup>1</sup>KEK/<sup>2</sup>JAEA, Tokai, Ibaraki, Japan

## Abstract

The J-PARC 3-GeV rapid cycling synchrotron has achieved a 1-MW beam operation with considerably low fractional beam loss of a couple of  $10^{-3}$ . Following this successful achievement, we have recently conducted further high-intensity beam tests toward a higher beam power beyond 1 MW. This paper reviews our continuous efforts for beam loss mitigation including the recent result of a 1.5-MW-equivalent high-intensity beam test.

## INTRODUCTION

The J-PARC 3-GeV rapid cycling synchrotron (RCS) is a world leading high-power pulsed proton driver, which has the goal of achieving a 1-MW beam power [1, 2]. A 400-MeV negative hydrogen ion ( $H^-$ ) beam from the injector linac is delivered to the RCS injection point, where it is multiturn charge-exchange injected through a carbon foil over a period of 0.5 ms (307 turns). The RCS accelerates the injected protons up to 3 GeV with a repetition rate of 25 Hz. Most of the RCS beam pulses are delivered to the materials and life science experimental facility (MLF), while only four pulses every several seconds (2.48 s or 5.2 s) are injected to the main ring (MR) by switching the beam destination pulse by pulse.

Figure 1 shows the history of the RCS beam power. In 2015, the beam power reached 500 kW. But it caused premature failures of the neutron production target two times in a row as shown by white arrows in Fig. 1, so that the beam power was reduced to 150–200 kW to prioritize availability for users. In 2017, a new improved target was installed. Since then, the beam power has been stepped up again while carefully monitoring the durability of the target. It now reaches 740 kW. If there are no unexpected troubles with the target from now on, the routine beam power will reach nearly 1 MW in two years.

Thus, we are still in the course of gradually increasing the beam power to 1 MW, but the accelerator itself has already well established a 1-MW beam operation. The most important issues in realizing such a MW-class high-power beam operation are controlling and minimizing beam loss, which are essential for sustainable beam operation that allows hands-on maintenance [3].

In high-power machines such as the RCS, there exist many factors causing beam loss, such as space charge, lattice imperfections and foil scattering. Besides, beam loss generally occurs through a complex mechanism involving several factors. In the RCS, numerical simulations have played a vital role in solving beam loss issues in combination with actual beam experiments; various ideas for beam loss mitigation were proposed with the

help of the numerical simulations, and verified by experiments. As a result of such continuous efforts including several hardware improvements, we have recently accomplished a 1-MW beam acceleration with considerably low fractional beam loss of several  $10^{-3}$  [4, 5].

This paper reviews our approaches to beam loss issues that we faced in the course of beam power ramp-up. Our recent efforts to further beam power ramp-up beyond 1 MW are also presented.

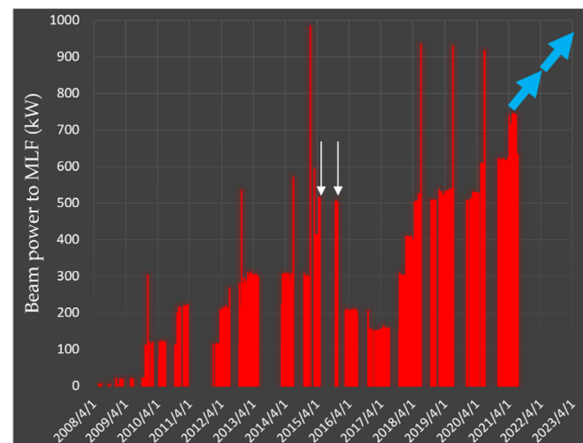


Figure 1: History of the RCS beam power.

## REVIEW OF BEAM TUNING FOR BEAM LOSS MITIGATION

### Beam Loss Mitigation by Injection Painting

In high-intensity proton synchrotrons, space charge in the low-energy region is one of the most crucial sources of beam loss. To mitigate this, the RCS adopts transverse and longitudinal injection painting.

In transverse injection painting [6], the phase space offsets between the centroid of the injection beam and the ring closed orbit are varied during multi-turn injection. By this way, the injection beam is uniformly distributed over a required phase-space area. On the other hand, in longitudinal injection painting [7, 8], a momentum offset to the rf bucket is introduced during multi-turn injection. In this way, a uniform bunch distribution is formed through emittance dilution by a large synchrotron motion excited by the momentum offset. In addition, the second harmonic rf and its phase sweep are introduced, which enable further bunch distribution control through a dynamical change of the rf bucket potential. By this way, the charge density peak in the longitudinal direction is effectively reduced.

Figure 2 shows the beam survival rates measured without and with the injection painting. In the case with no

† email address hideaki.hotchi@j-parc.jp

Content from this work may be used under the terms of the CC BY 3.0 licence (© 2021). Any distribution of this work must maintain attribution to the author(s), title of the work, publisher, and DOI

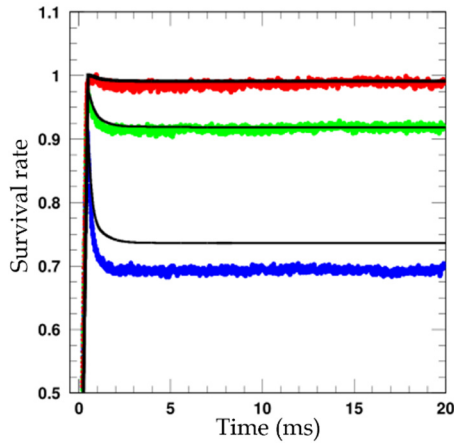


Figure 2: Beam survival rates measured without painting (blue), with longitudinal painting (green), and with transverse and longitudinal painting (red). The black solid curves show the numerical simulation results.

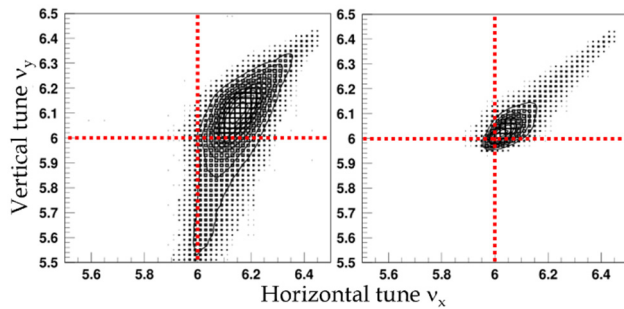


Figure 3: Numerical simulation results; tune footprints at the end of injection calculated without (left) and with injection painting (right).

painting, a critical 30% beam loss occurred in the low-energy region, where space charge is most serious. But the beam loss was drastically mitigated by the combination of the transverse and longitudinal painting. Figure 3 shows the tune footprints at the end of injection simulated without and with the injection painting. In the case with no painting, a core part of the beam particles crosses the integers ( $\nu_{x,y}=6$ ) due to the large space-charge detuning. On the integers, all-order systematic resonances are excited. The 30% large beam loss is ascribed to large emittance growth caused by the stopbands. As shown in Fig. 3, the injection painting well decreases the space-charge detuning. This mitigates the effect of the stopbands, as a result, leading to the significant beam loss reduction. This experiment clearly demonstrated the excellent ability of the injection painting for space-charge mitigation [4].

### Approach to Solving Beam Loss Issue Caused by the Combined Effect of Image Charge and Dipole Field Ripple

By introducing injection painting, the beam loss was drastically reduced as mentioned above, but there still remained nonnegligible beam loss of  $\sim 2\%$ , as shown in

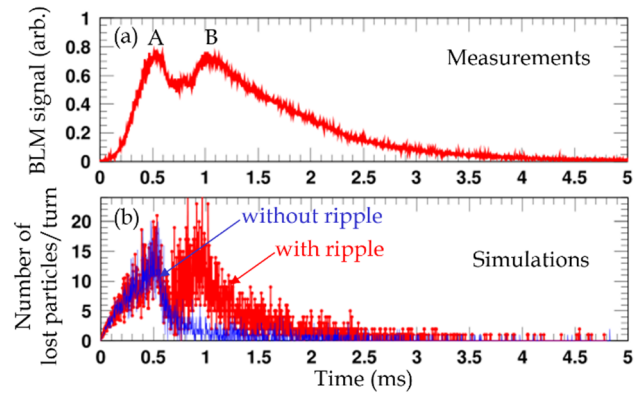


Figure 4: (a) Experimental result; time structure of beam loss. (b) Corresponding numerical simulation results.

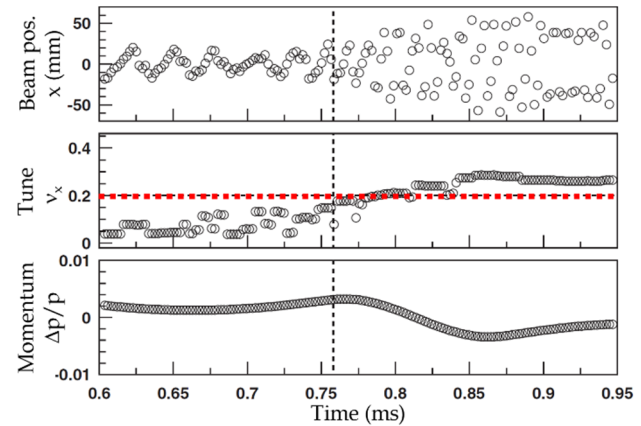


Figure 5: Numerical simulation result; single-particle motion near the resonance.

Fig. 4 (a). Further reduction of this beam loss was the next subject in our beam study. As shown in Fig. 4 (a), the beam loss consists of two peak structures; (A) and (B). The first beam loss (A) is caused by foil scattering during charge exchange injection. This is a very simple beam loss mechanism. On the other hand, the second beam loss (B) has a relatively complex mechanism. This beam loss is caused by a beam oscillation induced by a dipole field ripple [9], but it cannot be explained only by the presence of the beam oscillation. For understanding the beam loss mechanism, we have to additionally consider the effect of the image charge of the beam; the numerical simulation suggested that the beam loss (B) is caused by a betatron resonance driven by the combined effect of the beam oscillation and the image charge [4].

The image charge has a simple defocusing effect on a beam particle, but the strength varies depending on the square of the beam position. Thus, if the beam position oscillation is excited, the defocusing effect of the image charge periodically varies with two times higher frequency than that of the beam position oscillation. The oscillating defocusing force drives a second-order resonance, affecting the beam.

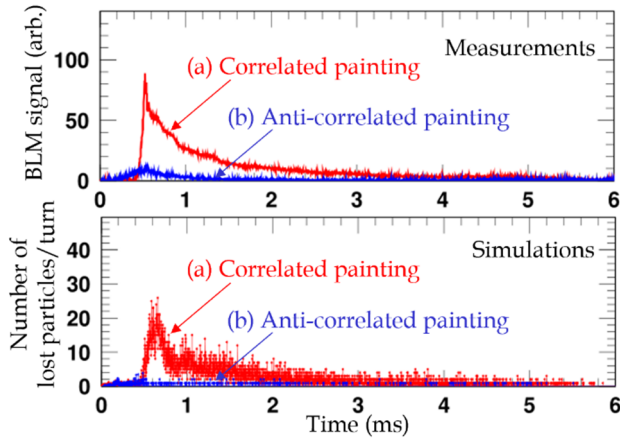


Figure 6: (Upper) Experimental results; time structure of beam loss. (Lower) Corresponding numerical simulation results.

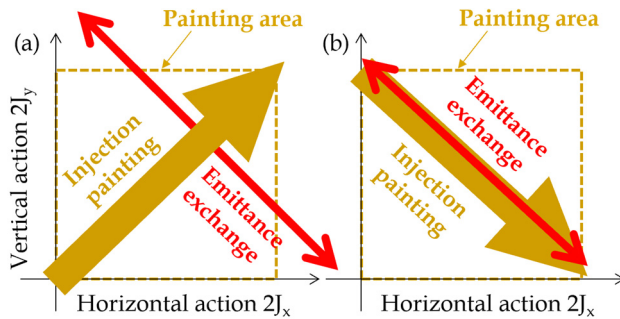


Figure 7: (a) Schematic of the geometrical relationship between correlated painting and emittance exchange in the  $(J_x, J_y)$  space. (b) Similar schematic for anti-correlated painting.

Figure 5 shows the motion of a beam particle near the resonance. The frequency of the beam position oscillation is  $\sim 100$  kHz, which corresponds to  $\sim 0.2$  in the wavenumber per turn, so that the resonance is excited at 0.2 in the betatron tune space. In Fig. 5, one can find that the amplitude of the betatron motion of the beam particle sharply increases when the betatron tune gets on the resonance. The beam loss (B) is ascribed to a beam halo formation caused by the resonance.

As shown in Fig. 4 (b), the experimental beam loss was well reproduced by the numerical simulation by including the measured dipole field ripple and also by considering the realistic boundary condition. The characteristic of this resonance is that it is an intensity-dependent phenomenon, and that it occurs at unusual betatron frequency depending on the frequency of the beam position oscillation. Receiving this study result, the power supply of the injection bump magnets, which was the source of the dipole field ripple, was improved. As a result, the dipole field ripple was drastically reduced, and the beam loss (B) was successfully removed [4].

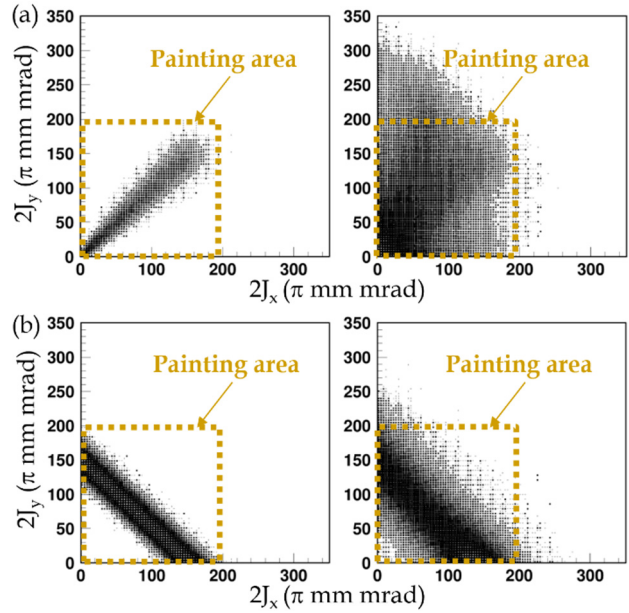


Figure 8: Numerical simulation results; scatter plots between the horizontal and vertical actions at the end of injection calculated without (left) and with (right) space charge. The upper (a) is for correlated painting, while the lower (b) is for anti-correlated painting.

### Approach to Solving Beam Loss Issue Caused by the Montague Resonance

The next subject in our beam study was to further reduce the residual beam loss coming from foil scattering during injection. The foil scattering beam loss occurs in proportion to the foil hitting rate during injection. One possible solution to reduce the foil hitting rate is to expand the transverse painting area, which serves to more quickly move the circulating beam away from the foil. The original painting area was  $100\pi$  mm mrad. In this case, the average number of foil hits per particle is as large as 20.0. This number can be reduced by  $\sim 1/4$  if the painting emittance is doubly enlarged. But it was not so easy to expand the painting area.

By introducing a large painting of  $200\pi$  mm mrad, the foil scattering beam loss was well reduced as expected, but another significant beam loss occurred as shown by (a) in the upper panel of Fig. 6. But the numerical simulation provided a clue to solve this issue. As shown by (a) in the lower panel of Fig. 6, the numerical simulation well reproduced the experimental beam loss and clearly showed that the beam loss is caused by the Montague resonance,  $2\nu_x - 2\nu_y = 0$  [10]. This resonance is excited mainly by the nonlinear space-charge field, causing emittance exchange between the horizontal and vertical planes.

Figure 7 (a) shows a 2d space of the horizontal and vertical actions, showing the mechanism of the beam loss. The yellow arrow shows the path of injection painting; the injection beam is painted from the middle to the outside on both the horizontal and vertical planes (called correlated painting). To this direction of injection painting,

Content from this work may be used under the terms of the CC BY 3.0 licence (© 2021). Any distribution of this work must maintain attribution to the author(s), title of the work, publisher, and DOI

the emittance exchange occurs in the orthogonal direction. Figure 8 (a) shows scatter plots of the horizontal and vertical actions at the end of injection calculated without and with space charge. In this figure, one can see that the beam particles are greatly diffused by the space charge, and some of them are greatly out of the painting area. The numerical simulation clearly showed that this diffusion of beam particles is caused by the emittance exchange ( $J_x$ - $J_y$  exchange of each particle) that occurs perpendicularly to the path of injection painting. This is the mechanism of the beam loss.

To solve this issue, the path of injection painting was modified as shown in Fig. 7 (b); the direction of vertical painting was reversed. That is, the injection beam is painted from the middle to the outside on the horizontal plane, but from the outside to the middle on the vertical plane (called anti-correlated painting). In this case, the direction of the injection painting is the same as that of the emittance exchange. This geometrical relationship between injection painting and emittance exchange has an advantage, which minimizes the diffusion of beam particles. In Fig. 8 (b), one can find that most of beam particles stay in the painting area though emittance exchange occurs, because the directions of the injection painting and the emittance exchange are the same.

As shown in Fig. 6, the beam loss was successfully reduced by changing the path of injection painting, as predicted by the numerical simulations [4]. By this effort, the painting area was doubly expanded with no additional beam loss, and thereby the foil scattering beam loss was sufficiently reduced.

### Mechanism of the Residual Beam Loss

By continuous efforts, the beam loss in the 1 MW beam operation was finally reduced to the order of  $10^{-3}$ , as shown by (b) in Fig. 6. The numerical simulation well reproduced the experimental beam loss, and found the residual beam loss mainly arises from the effect of  $3\nu_x=19$  driven by the sextupole field components intrinsic in the injection bump magnets [11].

As shown in Fig. 9, four sets of same-type pulsed dipole magnets, SB1-4, are utilized for forming a horizontal injection orbit bump of 93 mm; they are excited over 0.5 ms for multiturn injection and then sharply turned down within the next 0.35 ms. Figure 10 shows the measured field distributions of the SB 1, 2, 3, and 4 [12, 13]. In this figure, one can clearly see that each SB has a significant sextupole component.

Ideally, the SBs generate the same magnetic distribution except polarity. That is, the SB fields including the high-order field components cancel with each other through the integration over the SB1-4. In such an ideal case, the SB fields have no significant influence on the beam. But the actual situation is different from that. As shown in Fig. 9, the SBs are installed very close to each other. Besides, the distances of SB1-2 (SB3-4) and SB2-3 are different. Also, the SB1 and SB4 are very close to the quadrupole magnets. Due to such actual situations, each SB has a different magnetic interference with each nearby

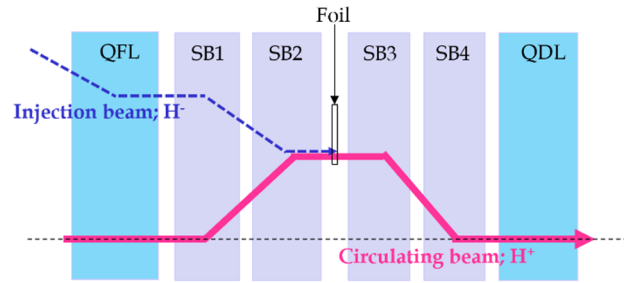


Figure 9: Schematic of the injection area.

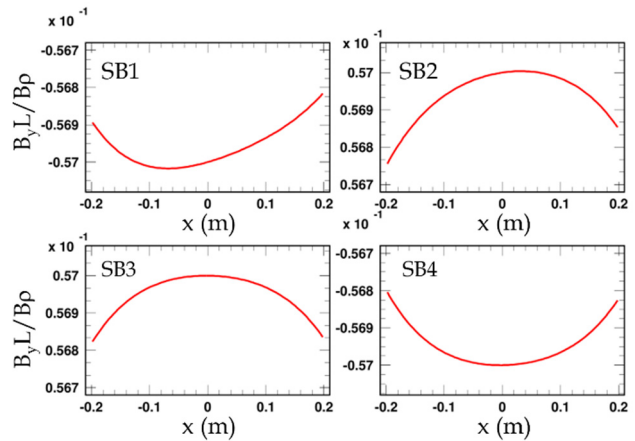


Figure 10: BL distributions ( $y=0$ ) measured for SB1-4.

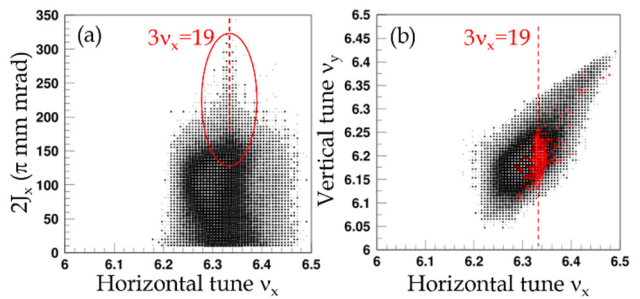


Figure 11: Numerical simulation results; (a) scatter plot of the horizontal tune and the horizontal action, and (b) tune footprint, calculated at the end of injection, where the particles painted red correspond to the beam halo particles found in (a).

component. Therefore, the actual field distributions of the SBs are not identical. In the actual beam operation, the SB fields are adjusted so that their dipole field components are compensated through the integration over the SB1-4. But, as to the higher-order field components, such a field compensation is incomplete due to the effects of the magnetic interferences. The residual sextupole component ( $K_2=0.012 \text{ m}^{-2}$ ), not cancels, excites the 3rd-order betatron resonance,  $3\nu_x=19$ .

Figure 11 (a) and (b) show the 2d plot of the horizontal tune and horizontal action and the tune footprint, calculated at the end of injection. In this figure, one can find that a horizontal beam halo is generated on the 3rd-order reso-

nance. This horizontal beam halo is the main cause of the residual beam loss. To correct the 3rd-order resonance, we need at least two sets of additional sextupoles with individual power supplies. But they are not urgent, because the residual beam loss is already small sufficiently.

### Demonstration of 1 MW Beam Operation

The amount of the residual beam loss in the 1-MW beam operation is as low as the order of  $10^{-3}$ . It is concentrated in the injection energy region, most of which is well localized at the collimator section. Under this condition, we performed a  $\sim 2$ -day continuous 1-MW beam operation at 25 Hz for users right before the summer maintenance period in 2020. During this beam operation, no serious issues were found. Besides, no unexpected increases in the residual radiation levels were found; the machine activations in the RCS were still maintained at sufficiently low levels of  $<80 \mu\text{Sv/h}$  at the injection area,  $<350 \mu\text{Sv/h}$  at the collimator area, and  $<3 \mu\text{Sv/h}$  at the high dispersion area, which were measured at 30 cm, 5 hours after the beam stop. Now we can say the accelerator itself including the linac is ready for the routine 1-MW beam operation.

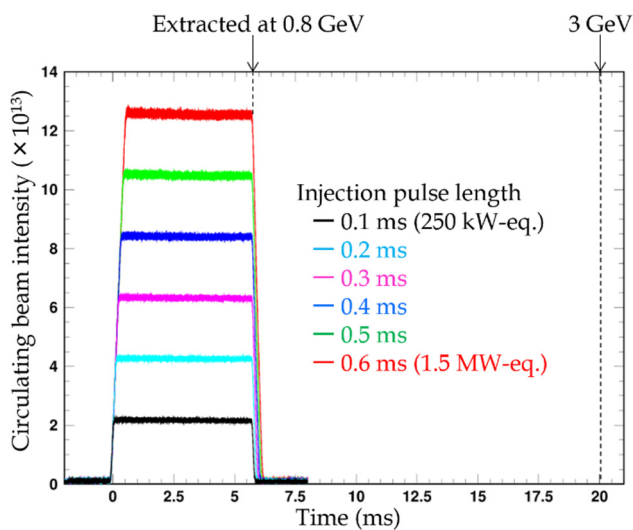


Figure 12: Experimental results; circulating beam intensities from injection to extraction.

### 1.5-MW BEAM TEST

The successful achievement of the low-loss 1-MW beam operation opened the door to further beam power ramp-up beyond 1 MW [4, 5].

We have recently performed a further high-intensity beam test by increasing both injection peak current (50 mA to  $>60$  mA) and injection pulse length (0.5 ms to 0.6 ms). The beam intensity reached  $1.26 \times 10^{14}$  particles per pulse, which corresponds to 1.5 MW at 3 GeV and 25 Hz. Due to the limitation of the ring RF system, the full acceleration of up to 3 GeV was not reached, but we achieved a 0.8 GeV acceleration for the high-intensity beam. Beam loss usually occurs for low energy region

below 0.8 GeV, so that we were able to complete sufficient beam loss studies even under the limited situation.

Figure 12 shows the result of the high-intensity beam test, showing the circulating beam intensity from injection to extraction, where the red one shows the maximum beam intensity which corresponds to 1.5 MW. In this figure, one can find that there is no significant beam loss; it's almost flat from injection to extraction. The beam loss in the low energy region, which was the most concern, was successfully reduced to the order of  $10^{-3}$  even for the 1.5-MW-equivalent high-intensity beam.

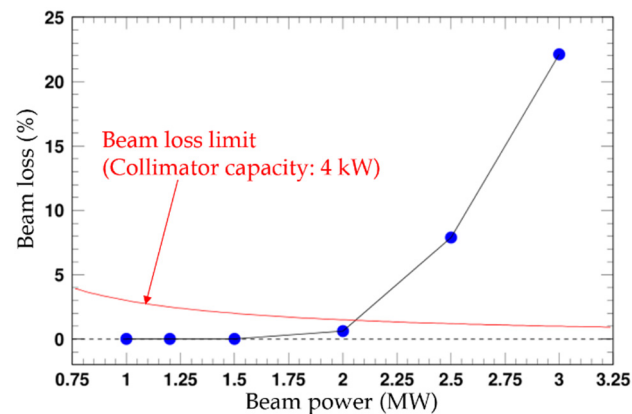


Figure 13: Numerical simulation results; intensity dependence of beam loss from 1 MW to 3-MW-equivalent intensity.

To realize the actual 1.5-MW beam operation, we need several hardware upgrades, such as the upgrade of the ring RF system [14]. But this experiment clearly demonstrated that the J-PARC RCS has a sufficient potential to realize a higher-power beam operation beyond 1 MW. The numerical simulation, which is displayed in Fig. 13, also supports the experimental result; it suggests the possibility of a low-loss 2-MW beam operation [5]. Looking ahead to future upgrades of J-PARC including the construction of the second target station, we will continue high-intensity beam studies aiming for a 1.5–2 MW beam power.

### SUMMARY

We are still in the course of gradually increasing the beam power to 1 MW while carefully monitoring the durability of the neutron production target, but the accelerator itself is ready for the routine 1-MW beam operation. By continuous efforts for beam loss mitigation including several hardware improvements, we have recently established a 1-MW beam operation with considerably low fractional beam loss of the order of  $10^{-3}$ . This beam loss amount corresponds to  $<1/10$  the typical value in the previous high-intensity proton synchrotrons. This achievement of the low-loss 1-MW beam operation opened the door to further beam power ramp-up beyond 1 MW. We are now

developing high-intensity beam tests toward achieving a 1.5-MW beam power or more with promising results.

## REFERENCES

- [1] High-intensity Proton Accelerator Project Team, J-PARC, JAERI Report, No. JAERI-Tech 2003-044, 2003.
- [2] H. Hotchi *et al.*, “Beam commissioning of the 3-GeV rapid cycling synchrotron of the Japan Proton Accelerator Research Complex”, *Phys. Rev. ST Accel. Beams*, vol. 12, p. 040402, Apr. 2009.  
doi:10.1103/PhysRevSTAB.12.040402
- [3] H. Hotchi, “High-power proton accelerators for pulsed spallation neutron sources”, *AAPPS Bull.*, vol. 31, p. 23, Oct. 2021. doi:10.1007/s43673-021-00025-0
- [4] H. Hotchi *et al.*, “Achievement of a low-loss 1-MW beam operation in the 3-GeV rapid cycling synchrotron of the Japan Proton Accelerator Research Complex”, *Phys. Rev. Accel. Beams*, vol. 20, p. 060402, Jun. 2017.  
doi:10.1103/PhysRevAccelBeams.20.060402
- [5] H. Hotchi *et al.*, “J-PARC 3-GeV RCS: 1-MW beam operation and beyond”, *JINST*, vol. 15, p. P07022, Jul. 2020.  
doi:10.1088/1748-0221/15/07/P07022
- [6] H. Hotchi *et al.*, “Beam loss reduction by injection painting in the 3-GeV rapid cycling synchrotron of the Japan Proton Accelerator Research Complex”, *Phys. Rev. ST Accel. Beams*, vol. 15, p. 040402, Apr. 2012.  
doi:10.1103/PhysRevSTAB.15.040402
- [7] F. Tamura *et al.*, “Longitudinal painting with large amplitude second harmonic rf voltages in the rapid cycling synchrotron of the Japan Proton Accelerator Research Complex”, *Phys. Rev. ST Accel. Beams*, vol. 12, p. 041001, Apr. 2009. doi:10.1103/PhysRevSTAB.12.041001
- [8] M. Yamamoto *et al.*, “Simulation of longitudinal beam manipulation during multi-turn injection in J-PARC RCS”, *Nucl. Instrum. Methods*, vol. 621, p. 15, 2010.  
doi:10.1016/j.nima.2010.04.050
- [9] Y. Shobuda *et al.*, “Analytical method for the evaluation of field modulation inside the rf-shielded chamber with a time-dependent dipole magnetic field”, *Phys. Rev. ST Accel. Beams*, vol. 12, p. 032401, Mar. 2009.  
doi:10.1103/PhysRevSTAB.12.032401
- [10] H. Hotchi, “Effects of the Montague resonance on the formation of the beam distribution during multiturn injection painting in a high-intensity proton ring”, *Phys. Rev. Accel. Beams*, vol. 23, p. 050401, May 2020.  
doi:10.1103/PhysRevAccelBeams.23.050401
- [11] H. Hotchi *et al.*, “J-PARC RCS: high-order field components inherent in the injection bump magnets and their effects on the circulating beam during multi-turn injection”, *J. Phys. Conf. Ser.*, vol. 1350, p. 012102, 2019.  
doi:10.1088/1742-6596/1350/1/012102
- [12] T. Takayanagi *et al.*, “Measurements of the injection bump magnets at J-PARC 3 GeV RCS”, in *Proc. the 4th Annual Meeting of Particle Accelerator Society of Japan*, Wako, Japan, Aug. 2007, p. 85.
- [13] H. Harada *et al.*, “Modelling for the injection bump system at the J-PARC 3 GeV Rapid Cycling Synchrotron”, in *Proc. the 4th Annual Meeting of Particle Accelerator Society of Japan*, Wako, Japan, Aug. 2007, p. 88.
- [14] M. Yamamoto *et al.*, “Conceptual design of a single-ended MA cavity for J-PARC RCS upgrade”, *J. Phys. Conf. Ser.*, vol. 1067, p. 052014, 2018.  
doi:10.1088/1742-6596/1067/5/052014